Smart Structures and Systems, Vol. 6, No. 8 (2010) 975-989
DOI: http://dx.doi.org/10.12989/sss.2010.6.8.975

Exact analyses for two kinds of piezoelectric hollow cylinders with graded properties

Taotao Zhang*[1] and Zhifei Shi[2]

[1]*School of Transportation Science and Engineering, Beihang University, Beijing, 100191, P.R. China*
[2]*School of Civil Engineering, Beijing Jiaotong University, Beijing, 100044, P.R. China*

(Received October 29, 2009, Accepted April 8, 2010)

Abstract. Based on the theory of piezo-elasticity, the paper obtains the exact solutions of functionally graded piezoelectric hollow cylinders with different piezoelectric parameter g_{31}. Two kinds of piezoelectric hollow cylinders are considered herein. One is a multi-layered cylinder with different parameter g_{31} in different layers; the other is a continuously graded cylinder with arbitrarily variable g_{31}. By using the Airy stress function method with plane strain assumptions, the exact solutions of the mechanic and electrical components of both cylinders are obtained when they are subjected to external voltage (actuator) and pressure (sensor), simultaneously. Furthermore, good agreement is achieved between the theoretical and numerical results, and useful conclusions are given.

Keywords: functionally graded material (FGM); ring actuator; multi-layered; piezoelectric material.

1. Introduction

Piezoelectric material is one of the most commonly used materials currently being investigated for the applications of smart structures due to its direct and converse piezoelectric effects, which permit it to be utilized as both sensors and actuators. Piezoelectric laminates, such as bimorphs or stacking structures, are the most common types for the application (Ikeda 1990, Crawley 1994). However, for a piezoelectric laminate with homogeneous material properties in layers, high stress concentrations generally exist at the layer interfaces under mechanical or electric loading, which may lead to lifetime limitations. To reduce the drawbacks, piezoelectric materials and structures with functionally graded material (FGM) properties in the direction of layer thickness have been proposed and fabricated (Zhu and Meng 1995, Wu *et al*. 1996, Taya *et al*. 2003, Ichinose *et al*. 2004). For optimal design and fabrication of the functionally graded piezoelectric material (FGPM) with desired properties, predicting and understanding the relationship between its compositional gradient and electro-mechanical response is of primary importance, which has attracted researchers' increasing attentions.

According to the literature, most of the previous studies are focused on modeling flat piezoelectric actuators. Kruusing (2000) provided the solution of a cantilever with graded material properties; a brief review of the design and simulation was also given based on the theory of primary elasticity. Using a simple analytical model, Hauke *et al*. (2000) investigated a kind of multi-morph piezoelectric actuator

*Corresponding Author, Assistant Professor, E-mail: zhangtt@buaa.edu.cn

and predicted the behavior of these functionally graded material (FGM) actuators. In Hauke's investigation, the bending actuator consists of N layers and the piezoelectric coefficient d_{31} in each layer satisfies the stepwise linear relationship. But all the other material parameters are assumed to be constants. The experimental results on BaTiO3 ceramics showed that the tip deflection of the actuator was slightly smaller than the case when the piezoelectric coefficient d_{31} in each layer keeps constant; however, the internal stresses were significantly reduced. For several kinds of functionally graded piezoelectric cantilevers and different loading cases, some analytical methods were presented and a set of exact solutions were obtained (Shi 2002, Liu and Shi 2004, Shi and Chen 2004, Shi 2005). The investigation on the linearly graded flat actuator showed that there is no stress component in the actuator when subjected to external voltage (Hauke *et al*. 2000). But some non-zero stress components are found in a curved actuator under the same loading condition (Shi 2005).

Numerous achievements have been made in the investigations of functionally graded flat sensors and actuators. During the last one to two decades, curved piezoelectric elements have attracted attentions in engineering applications. For example, due to the complicated shape of the bonding layer between a flat sensor/actuator and the curved surface of a host, it could be much more difficult to obtain the precise information for a tested point. In these cases, curved sensors and actuators have advantages over other flat piezoelectric devices. Now, curved sensors and actuators have found wide applications in engineering such as speakers for active noise control (Jayachandran *et al.* 1999) or active reflectors for space based satellite aperture antenna (Angelino and Washington 2002). Liu and Taciroglu (2007) established a method to quantify Saint-Venant's principle for laminated piezoelectric circular cylinders by using this method, the end effects for the displacements and voltages, as well as the stressed and electric displacements of the self-equilibrated states, are investigated. Yang (2007) presented a set of one-dimensional equations for coupled extension, flexure and shear of a planar piezoelectric curved bar, which are very useful in the analysis and design of one-dimensional piezoelectric curved devices. Larson and Vinson (1993) investigated the overall behaviors of shell composite laminas, each of which was composed of a piezoelectric laminate. Tzou and Gadre (1989) gave a detailed theoretical analysis of the vibration control of a multi-layered thin shell coupled with piezoelectric actuators. Based on the elastic theory, Zhang and Shi (2006) and Shi and Zhang (2008) discussed the bending behavior of functionally graded piezoelectric curved beams with different graded properties and gave their exact solutions, which is helpful for design and optimization of the piezoelectric transducers. Using Love's theory for thin shells, Chaudhry *et al*. (1994) and Sonti and Jones (1996) derived the static equivalent forces exerted by the collocated actuators on a cylinder. Rossi *et al*. (1993) investigated the actuation authority of collocated curved piezoelectric patches on a ring based on the impedance method (1996), which was experimentally verified by Lalande *et al.* (1995).

This paper aims to obtain the exact solutions of functionally graded piezoelectric hollow cylinder with different piezoelectric parameter g_{31} and validate the exact solutions by comparing to the numerical results. The rest of the paper is organized as follows. In Section 2, the basic equations which will be utilized for the derivation are given; in section 3 and section 4, two different kinds of piezoelectric hollow cylinders are considered, respectively. One is a multi-layered cylinder with different parameter g_{31} in different layer; another is a continuously graded cylinder with arbitrarily variable g_{31}. By using the Airy stress function method based on the theory of piezo-elasticity, the exact solutions of both mechanic and electrical components of the above two kinds of cylinders are obtained when simultaneously subjected to external voltage (actuator) and pressure (sensor), which is helpful for the research of the contact problems of piezoelectric devices. This is the major difference from the authors' previous work Zhang and Shi (2006) and

Shi and Zhang (2008). Furthermore, in Section 5, good agreement is achieved between the theoretical and numerical results and useful conclusions are given.

2. Basic equations

For the analysis of the piezoelectric curved actuator, the polar coordinate system (r, θ) will be used. Symbols S_{ij}, T_{ij}, D_i and E_i ($i, j = r$ or θ) denote the strain tensor, stress tensor, electric displacement and electric field, respectively. Without consideration of the body force and body charge, the elastic equilibrium and electrostatic equations are given by

$$\begin{cases} \dfrac{\partial T_r}{\partial r}+\dfrac{1}{r}\dfrac{\partial T_{r\theta}}{\partial \theta}+\dfrac{T_r-T_\theta}{r}=0 \\ \dfrac{\partial T_{r\theta}}{\partial r}+\dfrac{1}{r}\dfrac{\partial T_\theta}{\partial \theta}+\dfrac{2T_{r\theta}}{r}=0 \end{cases}, \quad \frac{1}{r}\frac{\partial D_\theta}{\partial \theta}+\frac{1}{r}D_r+\frac{\partial D_r}{\partial r}=0 \tag{1}$$

The constitutive equations of piezoelectric material under the plane strain condition can be written as

$$\begin{cases} S_\theta = s_{11}^D T_\theta + s_{13}^D T_r + g_{31} D_r \\ S_r = s_{13}^D T_\theta + s_{33}^D T_r + g_{33} D_r \\ S_{r\theta} = s_{44}^D T_{r\theta} + g_{15} D_\theta \end{cases}, \quad \begin{cases} E_\theta = -g_{15} T_{r\theta} + \zeta_{11} D_\theta \\ E_r = -g_{31} T_\theta - g_{33} T_r + \zeta_{33} D_r \end{cases} \tag{2}$$

where s_{ij}^D, g_{ij} and ζ_{ij} are the effective elastic compliance, piezoelectric and dielectric impermeability, respectively. The relationships of the strain and electric field with the displacement components (u_r and u_θ) and electrical potential (ϕ), respectively, are as follows

$$\begin{cases} S_\theta = \dfrac{u_r}{r}+\dfrac{1}{r}\dfrac{\partial u_\theta}{\partial \theta} \\ S_r = u_{r,r} \\ S_{r\theta} = \dfrac{1}{r}\dfrac{\partial u_r}{\partial \theta}+\dfrac{\partial u_\theta}{\partial r}-\dfrac{u_\theta}{r} \end{cases}, \quad \begin{cases} E_\theta = -\dfrac{1}{\mathrm{r}}\dfrac{\partial \phi}{\partial \theta} \\ E_r = -\dfrac{\partial \phi}{\partial r} \end{cases} \tag{3}$$

Moreover, in order to ensure that displacement can be found by integrating the strain field, strains must satisfy the following compatibility equation

$$\left(\frac{\partial^2}{\partial r^2}+\frac{2}{r}\frac{\partial}{\partial r}\right)S_\theta+\left(\frac{1}{r^2}\frac{\partial^2}{\partial \theta^2}-\frac{1}{r}\frac{\partial}{\partial r}\right)S_r = \left(\frac{1}{r^2}\frac{\partial}{\partial \theta}+\frac{1}{r}\frac{\partial^2}{\partial r \partial \theta}\right)S_{r\theta} \tag{4}$$

Solutions of the above equations for different kinds of piezoelectric curved actuators will be provided in the following sections. Note that the dielectric and elastic coefficients are related to the degree of polling as demonstrated by some experimental investigations; however, their dependence on polling is much less pronounced than that of the piezoelectric coefficients g_{31} in *Type-g* or d_{31} in *Type-d* constitutive equations (Hauke *et al*. 2000, Marcus 1984, Kouvatov *et al*. 1999). Therefore in this paper, the dielectric and elastic coefficients are assumed to be constants except the piezoelectric coefficient g_{31}.

3. Bending behavior of the multi-layered piezoelectric hollow cylinder

Fig. 1 shows the piezoelectric multi-layered hollow cylinder with inner surface being fixed. It is assumed that all layers are polarized in radial direction. Between the outer and inner surfaces of the actuator, an electrical voltage V_0 and external force q are applied. Considering that the piezoelectric parameter g_{31} plays an important part in the evaluation of the behavior of piezoelectric materials and the performances of piezoelectric products, many investigations have been made on the properties of the piezoelectric materials with different values of g_{31}. In the present analysis, different g_{31} in different layers will be considered. For convenience, the piezoelectric coefficient g_{31} of the i-th layer is denoted as g_{31i} (i=1~N). Without loss of generality, other piezoelectric, dielectric and elastic coefficients are assumed to be constants for all the layers.

3.1 Solutions of the basic equations

To obtain the solutions of the above basic equations, *Airy* stress function $\Psi(r)$ is introduced and one has

$$T_r = \frac{\Psi'(r)}{r}, \quad T_\theta = \Psi''(r), \quad T_{r\theta} = 0 \tag{5}$$

Furthermore, the electrical potential is assumed to be a function of the radius r only, i.e., $\phi = \phi(r)$. Keeping the third expression in Eq. (5) in mind, the following electrical field can be obtained from Eqs. (1)-(3)

$$E_\theta = 0, \quad D_\theta = 0, \quad E_r = -\phi'(r), \quad D_r = \frac{C_5}{r} \tag{6}$$

where C_5 is a constant to be determined. Using Eqs. (2) and (4)-(6), *Airy* stress function $\Psi(r)$ can be obtained as follows

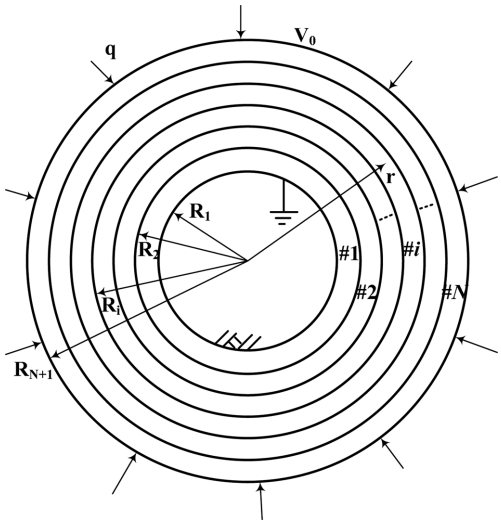

Fig. 1 Schematic of the cross-section of the multi-layered piezoelectric cylinder

$$\Psi(r) = -Gr + C_1 + C_2 r^2 + C_3' r^{(-S+1)} + C_4' r^{S+1} \tag{7}$$

where C_i (i=1~4) are undetermined constants. Based on the theory of elasticity, it can be easily understood that C_1 needs not to be considered because it has no influence on the elastic field.

Substituting Eq. (7) into Eq. (5), the stress components can then be calculated by

$$\begin{cases} T_\theta = \Psi''(r) = 2C_2 - C_3' S(-S+1) r^{-S-1} + C_4' S(S+1) r^{S-1} \\ T_r = \dfrac{\Psi'(r)}{r} = -\dfrac{G}{r} + 2C_2 + C_3'(-S+1) r^{-S-1} + C_4'(S+1) r^{S-1} \end{cases} \tag{8}$$

in which

$$G = \frac{g_{33} C_5}{s_{33}^D}, \quad S = \sqrt{\frac{s_{33}^D}{s_{11}^D}} \tag{9}$$

Finally, the displacement and electrical potential components can be obtained by using Eqs. (2) and (3)

$$\begin{cases} u_r = s_{13}^D [2C_2 r + C_3'(-S+1) r^{-S} + C_4'(S+1) r^S] - (G S_{13}^D - g_{31} C_5) \\ \qquad + s_{33}^D \left[2C_2 r - C_3' \dfrac{-S+1}{S} r^{-S} + C_4' \dfrac{S+1}{S} r^S\right] + P_1 \cos\theta + P_2 \sin\theta \\ u_\theta = 2C_2 (s_{11}^D - s_{33}^D) r\theta + P_2 \cos\theta - P_1 \sin\theta + r P_3 \end{cases} \tag{10}$$

$$\begin{aligned} \phi = {} & g_{31} [2C_2 r + C_3'(-S+1) r^{-S} + C_4'(S+1) r^S] - \zeta_{33} C_5 \ln r + C_6 \\ & + g_{33} \left[-G \ln r + 2C_2 r - C_3' \frac{-S+1}{S} r^{-S} + C_4' \frac{S+1}{S} r^S\right] \end{aligned} \tag{11}$$

in which P_1, P_2, P_3 and C_6 are constants to be determined. Eqs. (6), (8), (10) and (11) constitute one kind of solutions of the above basic equations, which can be used to study the bending behaviors of the piezoelectric curved multi-layered actuator.

Furthermore, for a piezoelectric hollow cylinder, the above equations can be simplified as follows according to the symmetrical characteristic and the fixed boundary condition at the inner surface

$$\begin{cases} T_\theta = \Psi''(r) = -C_3 S r^{-S-1} + C_4 S r^{S-1} \\ T_r = \dfrac{\Psi'(r)}{r} = -\dfrac{G}{r} + C_3 r^{-S-1} + C_4 r^{S-1} \end{cases} \tag{12}$$

$$\begin{cases} u_r = s_{13}^D [C_3 r^{-S} + C_4 r^S] - (G s_{13}^D - g_{31} C_5) + \dfrac{s_{33}^D}{S} [-C_3 r^{-S} + C_4 r^S] \\ u_\theta = 0 \end{cases} \tag{13}$$

$$\phi = g_{31} [C_3 r^{-S} + C_4 r^S] + \frac{g_{33}}{S} [-C_3 r^{-S} + C_4 r^S] - \left(\frac{g_{33}^2}{s_{33}^D} + \zeta_{33}\right) C_5 \ln r + C_6 \tag{14}$$

where

$$C_3 = C_3'(-S+1), \; C_4 = C_4'(S+1)$$

3.2 The exact solution of the multi-layered piezoelectric hollow cylinder

By assembling the equations above, the exact solution can be obtained for a piezoelectric multi-layered hollow cylinder as shown in Fig. 1. For convenience, the unknown constants in Eqs. (6), (12), (13) and (14) will be distinguished by (G_i, C_{ji}) (i =1~N; j = 2~6) corresponding to the i-th layer of the curved actuator respectively. In order to find the exact solution of the multi-layered actuator, certain boundary conditions and connecting conditions should be taken into account. First, the connecting condition of the electric displacement at the interface of any two adjacent layers ($D_r\big|_{r=R_{(i+1)+}} = D_r\big|_{r=R_{(i+1)-}}$, i=1~N-1) leads to

$$C_{51} = \ldots = C_{5i} = \ldots = C_5 \quad \text{or } G_1 = \ldots = G_i = \ldots = G \tag{15}$$

The boundary conditions of the electrical potential at the outer and inner surfaces satisfy the following two equations, respectively

$$g_{31N}[C_{3N}R_{N+1}^{-S} + C_{4N}R_{N+1}^{S}] + \frac{g_{33}}{S}[-C_{3N}R_{N+1}^{-S} + C_{4N}R_{N+1}^{S}] - (\frac{g_{33}^2}{s_{33}^D} + \zeta_{33})C_5 \ln R_{N+1} + C_{6N} = V_0 \tag{16}$$

$$g_{311}[C_{31}R_1^{-S} + C_{41}R_1^{S}] + \frac{g_{33}}{S}[-C_{31}R_1^{-S} + C_{41}R_1^{S}] - (\frac{g_{33}^2}{s_{33}^D} + \zeta_{33})C_5 \ln R_1 + C_{61} = 0 \tag{17}$$

The connecting condition of the electrical potential at the interface of any two adjacent layers ($\phi\big|_{r=R_{(i+1)+}} = \phi\big|_{r=R_{(i+1)-}}$, i=1~N-1) can be rewritten as

$$\begin{aligned} &g_{31i}[C_{3i}R_{i+1}^{-S} + C_{4i}R_{i+1}^{S}] + \frac{g_{33}}{S}[-C_{3i}R_{i+1}^{-S} + C_{4i}R_{i+1}^{S}] + C_{6i} \\ &= g_{31(i+1)}[C_{3(i+1)}R_{i+1}^{-S} + C_{4(i+1)}R_{i+1}^{S}] + \frac{g_{33}}{S}[-C_{3(i+1)}R_{i+1}^{-S} + C_{4(i+1)}R_{i+1}^{S}] + C_{6(i+1)} \end{aligned} \quad (i=1\sim N\text{-}1) \tag{18}$$

In this case, the mechanical boundary conditions $T_{r\theta}\big|_{r=R_1} = 0$ and $T_{r\theta}\big|_{r=R_{N+1}} = 0$ as well as the connecting conditions between any two conterminous layers $T_{r\theta}\big|_{r=R_{(i+1)+}} = T_{r\theta}\big|_{r=R_{(i+1)-}}$ (i=1~N-1) are automatically satisfied. Moreover, the boundary conditions $u_r\big|_{r=R_1}$=0 (the fixed end at $r = R_1$) and $T_r\big|_{r=R_{N+1}} = -q$ are equivalent to the following two equations, respectively

$$s_{13}^D[C_3R_1^{-S} + C_4R_1^{S}] - (Gs_{13}^D - g_{31}C_5) + \frac{s_{33}^D}{S}[-C_3R_1^{-S} + C_4R_1^{S}] = 0 \tag{19}$$

$$-GR_{N+1}^{-1} + C_{3N}R_{N+1}^{-S-1} + C_{4N}R_{N+1}^{S-1} = -q \tag{20}$$

The connecting conditions of the stress at the interface ($T_r\big|_{r=R_{(i+1)+}} = T_r\big|_{r=R_{(i+1)-}}$, i=1~N-1) can be expressed as

$$C_{3i}R_{i+1}^{-S-1} + C_{4i}R_{i+1}^{S-1} = C_{3(i+1)}R_{i+1}^{-S-1} + C_{4(i+1)}R_{i+1}^{S-1} \tag{21}$$

In addition, the displacement should be also continuous at any interface, i.e., $u_r\big|_{r=R_{(i+1)+}} = u_r\big|_{r=R_{(i+1)-}}$ the following equation

$$\begin{aligned} &s_{13}^{D}[C_{3i}R_{i+1}^{-S}+C_{4i}R_{i+1}^{S}]+\frac{s_{33}^{D}}{S}[-C_{3i}R_{i+1}^{-S}+C_{4i}R_{i+1}^{S}]+g_{31i}C_5 \\ &=s_{13}^{D}[C_{3(i+1)}R_{i+1}^{-S}+C_{4(i+1)}R_{i+1}^{S}]+\frac{s_{33}^{D}}{S}[-C_{3(i+1)}R_{i+1}^{-S}+C_{4(i+1)}R_{i+1}^{S}]+g_{31(i+1)}C_5 \end{aligned} \tag{22}$$

Utilizing the above eight equations (Eqs. (15)~(22)), the (3N+1) unknown constants C_{3i}, C_{4i}, C_{6i} and C_5 can be determined after tedious deduction. The relationship between C_{ij} (i=3, 4, 6; j=1~N) and C_5 can be obtained as follows

$$C_{31} = \Sigma_{31}C_5 + q_3 \tag{23a}$$

$$C_{41} = \Sigma_{41}C_5 + q_4 \tag{23b}$$

$$C_{61} = \Sigma_{61}C_5 + q_6 \tag{23c}$$

$$C_{ij} = q_i + \Sigma_{ij}C_5 \qquad (i=3,4\ j=2\sim N) \tag{23d}$$

$$C_{6j} = q_{6j} + \Sigma_{6j}C_5 \quad (j=2\sim N) \tag{23e}$$

where the following notations are introduced. When $N=1$

$$\Sigma_{31}=[(\Sigma_3(N)R_{N+1}^{-S}+\Sigma_4(N)R_{N+1}^{S}-\frac{g_{33}}{s_{33}^{D}})B+(\frac{g_{33}}{s_{33}^{D}}s_{13}^{D}-g_{311})R_{N+1}^{S}](AR_{N+1}^{S}-BR_{N+1}^{-S})^{-1} \tag{24a}$$

$$\Sigma_{41}=-[(\Sigma_3(N)R_{N+1}^{-S}+\Sigma_4(N)R_{N+1}^{S}-\frac{g_{33}}{s_{33}^{D}})A+(\frac{g_{33}}{s_{33}^{D}}s_{13}^{D}-g_{311})R_{N+1}^{-S}](AR_{N+1}^{S}-BR_{N+1}^{-S})^{-1} \tag{24b}$$

$$\Sigma_{61}=(\frac{g_{33}^{2}}{s_{33}^{D}}+\varsigma_{33})\ln R_1-(g_{311}-\frac{g_{33}}{S})\Sigma_{31}R_1^{-S}-(g_{311}+\frac{g_{33}}{S})\Sigma_{41}R_1^{S} \tag{24c}$$

$$q_3=qR_{N+1}B(AR_{N+1}^{S}-BR_{N+1}^{-S})^{-1} \tag{24d}$$

$$q_4=-qR_{N+1}A(AR_{N+1}^{S}-BR_{N+1}^{-S})^{-1} \tag{24e}$$

$$q_6=-(g_{311}-\frac{g_{33}}{S})q_3R_1^{-S}-(g_{311}+\frac{g_{33}}{S})q_4R_1^{S} \tag{24f}$$

$$\Sigma_{qj}=\sum_{i=1}^{j-1}\Delta_i(q_3R_{i+1}^{-S}+q_4R_{i+1}^{S}) \tag{24g}$$

$$q_{6j} = q_6 + \Sigma_{qj} \tag{24h}$$

$$A=(s_{13}^{D}-\frac{s_{33}^{D}}{S})R_1^{-S},\ \ B=(s_{13}^{D}+\frac{s_{33}^{D}}{S})R_1^{S} \tag{24i}$$

When $N\geq 2$, one has

$$\Sigma_{3j} = \Sigma_{31} + \Sigma_3(j) \tag{24j}$$

$$\Sigma_{4j} = \Sigma_{41} + \Sigma_4(j) \tag{24k}$$

$$\Sigma_{6j} = \Sigma_{61} + \sum_{i=1}^{j-1} \Delta_i (R_{i+1}^{-S} \Sigma_{3i} + R_{i+1}^{S} \Sigma_{4i} - \frac{g_{33}}{s_{33}^{D}}) \tag{24l}$$

$$\Delta_i = g_{31i} - g_{31(i+1)} \tag{24m}$$

$$\Sigma_3(j) = \frac{-S}{2s_{33}^{D}} \sum_{i=1}^{j-1} \Delta_i R_{i+1}^{S} \tag{24n}$$

$$\Sigma_4(j) = \frac{S}{2s_{33}^{D}} \sum_{i=1}^{j-1} \Delta_i R_{i+1}^{-S} \tag{24o}$$

Keeping Eq. (9) in mind and substituting Eq. (23) into Eq. (16), one can find the expression of C_5 as

$$C_5 = V' \cdot (\Sigma_N)^{-1} \tag{25}$$

in which

$$V' = V_0 + g_{31N} q R_{N+1} + \frac{g_{33}}{S}(q_3 R_{N+1}^{-S} - q_4 R_{N+1}^{S}) - q_{6N} \tag{26a}$$

$$\Sigma_N = \frac{g_{31N} g_{33}}{s_{33}^{D}} + \frac{g_{33}}{S}\left(-R_{N+1}^{-S} \Sigma_{3N} + R_{N+1}^{S} \Sigma_{4N}\right) - \left(\frac{g_{33}^{2}}{s_{33}^{D}} + \varsigma_{33}\right) \ln R_{N+1} + \Sigma_{6N} \tag{26b}$$

Substituting Eq. (25) into Eq. (23), all the unknown constants can be determined.

Thus, all the mechanical and electrical fields of the multi-layered piezoelectric cylinder have been obtained fully based on the theory of elasticity.

Table 1 lists the data of the elastic, piezoelectric and dielectric impermeability constants of PZT-4, which is transformed from Table 2 (Ruan *et al*. 2000). To perform a numerical calculation, consider a 5-layered curved actuator with the radius for each layer determined by $R_i = R_1 + (i - 1)\ R_{N+1} - R_1 / N (i = 1...6)$ as 16, 16.264, 16.528, 16.792, 17.056 and 17.32 mm. The piezoelectric coefficient g_{31} for each layer (g_{31i}, $i = 1 \ldots 5$) is assigned as -7×10^{-3}($BaTiO_3$), -9.5×10^{-3}, -11.5×10^{-3}, -13.8×10^{-3} and -17.8×10^{-3} m^2/C (PZT-4), respectively. With the applied external voltage $V_0 = 100$ V and external load $q = 10$ kN/m^2, Figs. 2-5 illustrate the variations of the normal stresses (T_r, T_θ), electrical potential ϕ and radical electric displacement D_r with respect to the radius r (solid lines). Fig. 6 shows the displacement u_r with respect to r under the same boundary conditions (solid lines). Fig. 7 shows the relationship

Table 1 Some material constants of PZT-4 (For Model-g constitutive relations)

Elastic constant (10^{-12} m^2/N)				Piezoelectric constant (10^{-3} m^2/C)			Dielectric impermeability constant (10^6 m/F)	
s_{11}^{D}	s_{13}^{D}	s_{33}^{D}	s_{44}^{D}	g_{31}	g_{33}	g_{15}	ζ_{11}	ζ_{33}
7.95	-3.03	7.91	17.91	-17.8	23.91	40.36	76.87	99.65

Table 2 Some material constants of PZT-4 (For Model-d constitutive relations)

Elastic constant (10^{-12} m^2/N)				Piezoelectric constant (10^{-12} C/N)			Dielectric impermeability constant	
s_{11}^{E}	s_{13}^{E}	s_{33}^{E}	s_{44}^{E}	d_{31}	d_{33}	d_{15}	ε_{11}^{T}	ε_{33}^{T}
12.4	-5.52	16.1	39.1	-135	300	525	1470	1300

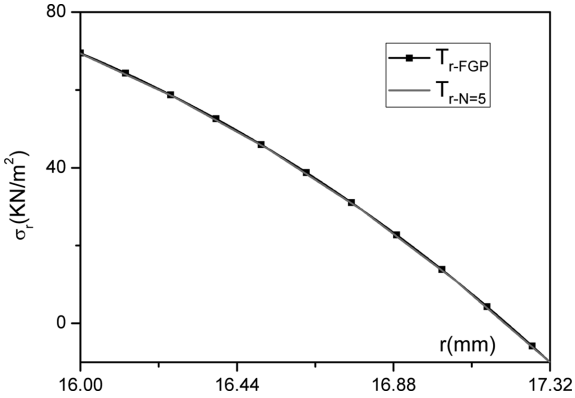

Fig. 2 Distribution of stress T_r along radial direction

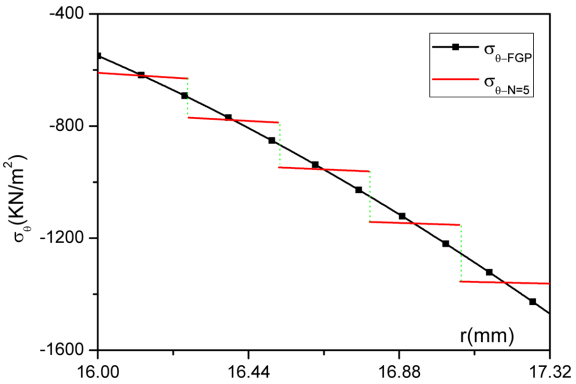

Fig. 3 Distribution of stress T_θ along radial direction

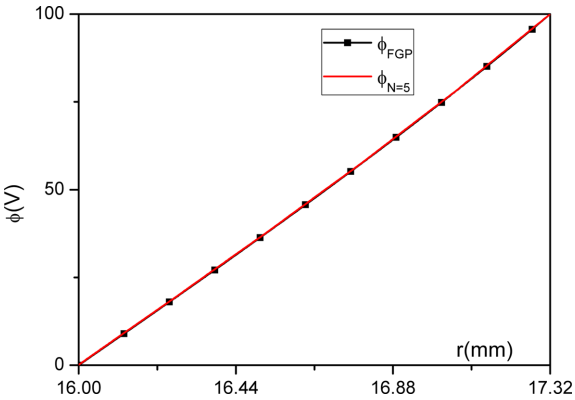

Fig. 4 Distribution of potential ϕ along radial direction

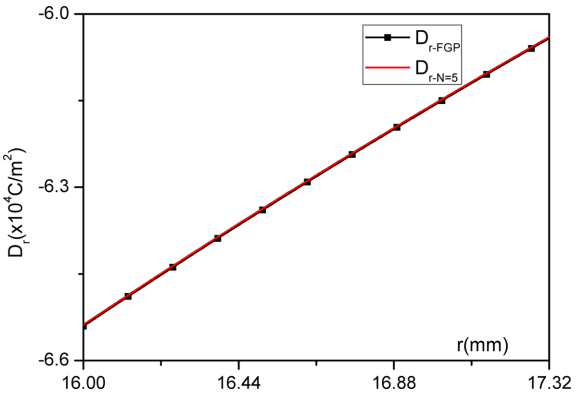

Fig. 5 Distribution of electric displacement D_r along radial direction

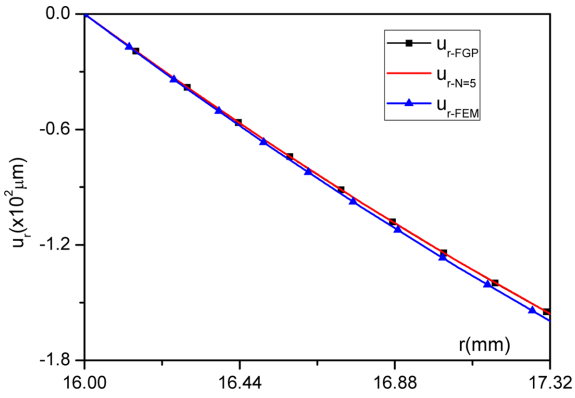

Fig. 6 Distribution of displacement u_r along radial direction

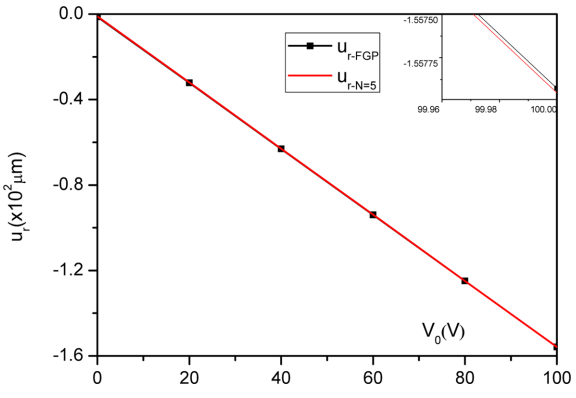

Fig. 7 Relationship between radial displacement u_r and external voltage V_0

between the tip deflection u_r and the applied electrical potential V_0 while the external load $q = 10$ kN/m^2 (solid lines). It is noted that in Figs. 2-7, the lines with square are functional graded piezoelectric (FGP) results which will be explained in Section 5.

4. Bending behavior of the piezoelectric hollow cylinder with generalized piezoelectric parameter

The functionally graded piezoelectric hollow cylinder with fixed end at the inner surface as shown in Fig. 8 is considered in this section. It is assumed that the actuator is polarized in radial direction. The electric potentials of the outer and inner surfaces are V_0 and 0, respectively. The pressure applied on the outer surface is q. In this section, the case that the piezoelectric parameter g_{31} has an arbitrary distribution (i.e., $g_{31} = g_{31}(r)$) is considered. Without loss of generality, all the material parameters except g_{31} are assumed as constants in the analysis. In order to find the solution, Taylor series expansion method is introduced and the arbitrary function $g_{31}(r)$ is expressed in terms of the following Kth order polynomial

$$g_{31}(r) = J_0 + J_1 r + J_2 r^2 + \ldots + J_K r^K = \sum_{i=0}^{K} J_i r^i \tag{27}$$

where J_i (i = 0...K) are the material constants. Eqs. (1)-(6) are still valid in this case. Using Eqs. (1)-(6), *Airy* stress function $\Psi(r)$ can be obtained as follows

$$\Psi(r) = -Gr + C_1 + C_2 r^2 + C_3' r^{(-S+1)} + C_4' r^{S+1} + f(r) C_5 \tag{28}$$

where

$$f(r) = \frac{1}{s_{11}^D} \sum_{i=2}^{K} \frac{i}{i+1} \frac{J_i}{S^2 - i^2} r^{i+1}, \quad G = \frac{g_{33} C_5}{s_{33}^D}, \quad S = \sqrt{\frac{s_{33}^D}{s_{11}^D}} \tag{29}$$

C_i(i = 1~5) are undetermined constants. Based on the theory of elasticity, C_1 needs not to be considered because it has no influence on the elastic field.

Substituting Eq. (28) into Eq. (5) and keeping in mind the symmetry of the cross section and the boundary conditions of the fixed end at the inner surface, the stress components can then be calculated by

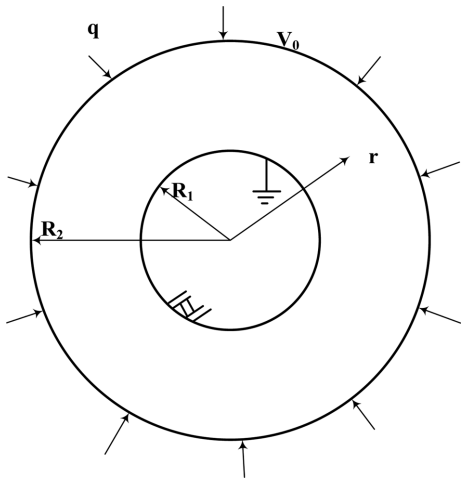

Fig. 8 Schematic of the cross-section of the continuously graded piezoelectric cylinder

$$\begin{cases} T_\theta = \Psi''(r) = -C_3 S r^{-S-1} + C_4 S r^{S-1} + \left(f''(r) + \dfrac{b(r)}{r} \right) C_5 \\ T_r = \dfrac{\Psi'(r)}{r} = -\dfrac{G}{r} + C_3 r^{-S-1} + C_4 r^{S-1} + \dfrac{f'(r) + b(r)}{r} C_5 \end{cases} \tag{30}$$

in which

$$f'(r) = \frac{1}{s_{11}^D} \sum_{i=2}^{K} i \frac{J_i}{S^2 - i^2} r^i, \quad f''(r) = \frac{1}{s_{11}^D} \sum_{i=2}^{K} i^2 \frac{J_i}{S^2 - i^2} r^{i-1} \tag{31}$$

The displacement and electric potential of the actuator can be found to be

$$\begin{cases} u_r = s_{13}^D [C_3 r^{-S} + C_4 r^S + (b(r) + f'(r)) C_5] - (G s_{13}^D - J_0 C_5) \\ \quad + s_{33}^D [-\dfrac{C_3}{S} r^{-S} + \dfrac{C_4}{S} r^S + (b(r) + f_2(r)) C_5] \\ u_\theta = 0 \end{cases} \tag{32}$$

$$\begin{aligned} \phi = & \sum_{i=0}^{K} \left[-\frac{C_3 J_i S}{i - S} r^{i-S} + \frac{C_4 J_i S}{i + S} r^{i+S} + C_5 b(r) \frac{J_i}{i+1} r^i \right] \\ & + C_5 f_3(r) + g_{33} [-G \ln r - \frac{C_3}{S} r^{-S} + \frac{C_4}{S} r^S + (b(r) + f_2(r)) C_5] - \zeta_{33} C_5 \ln r + C_6 \end{aligned} \tag{33}$$

where

$$b(r) = \frac{1}{s_{11}^D - s_{33}^D} [(J_0 - g_{31}(r)) + \sum_{i=2}^{K} J_i r^i], \quad 2C_2 = \frac{b(r)}{r} C_5 \tag{34}$$

$$f_2(r) = \frac{1}{s_{11}^D} \sum_{i=2}^{K} \frac{J_i}{S^2 - i^2} r^i, \quad f_3(r) = \frac{1}{s_{11}^D} \int \left(\sum_{i=2}^{K} i^2 \frac{J_i}{S^2 - i^2} r^{i-1} \sum_{i=0}^{K} J_i r^i \right) dr \tag{35}$$

It can be easily found that the electric displacement D_θ automatically satisfies the boundary conditions, and the shear stress automatically satisfies all the mechanical boundary conditions. Other mechanical and electrical boundary conditions can be expressed as follows

$$u_r\big|_{r=R_1} = 0, \; T_r\big|_{r=R_2} = -q, \; \phi\big|_{r=R_1} = 0, \; \phi\big|_{r=R_2} = V_0 \tag{36}$$

Keeping Eq. (9) in mind and using Eq. (12), the unknown constants C_3, C_4, C_5 and C_6 can be obtained as

$$C = H^{-1} L \tag{37}$$

in which

$$C = \begin{Bmatrix} C_3 \\ C_4 \\ C_5 \\ C_6 \end{Bmatrix}, H = \begin{pmatrix} A & B & l & 0 \\ R_2^{-S-1} & R_2^{S-1} & l_R & 0 \\ \Re_{31} & \Re_{41} & \Re_{51} & 1 \\ \Re_{32} & \Re_{42} & \Re_{52} & 1 \end{pmatrix}, L = \begin{Bmatrix} 0 \\ -q \\ 0 \\ V_0 \end{Bmatrix} \tag{38}$$

where

$$l_R = \frac{f'(R_2) + b(R_2) - \dfrac{g_{33}}{s_{33}^D}}{R_2} \tag{39a}$$

$$\Re_{3j} = -\frac{g_{33}R_j^{-S}}{S} - \sum_{i=0}^{K} S\frac{J_i}{i-S}R_j^{i-S} \quad (j=1,2) \tag{39b}$$

$$\Re_{4j} = \frac{g_{33}R_j^{-S}}{S} + \sum_{i=0}^{K} S\frac{J_i}{i+S}R_j^{i+S} \tag{39c}$$

$$\Re_{5j} = f_3(R_j) + g_{33}(b(R_j) + f_2(R_j)) - (\frac{g_{33}^2}{s_{33}^D} + \varsigma_{33})\ln R_j + \sum_{i=0}^{K} b(R_j)\frac{J_i}{i+1}R_j^i \tag{39d}$$

$$l = \left(s_{13}^D + s_{33}^D\right)b(R_1) + s_{13}^D f'(R_2) + s_{33}^D f_2(R_2) - (\frac{g_{33}^2}{s_{33}^D}s_{13}^D - J_0) \tag{39e}$$

Thus, all the mechanical and electrical fields of the curved actuator with arbitrary distribution of the piezoelectric parameter g_{31} have been obtained.

The numerical and parametric analyses are performed as the next step to verify the obtained analytical solutions. In this case study, an exponential function is assumed for the piezoelectric parameter g_{31} as follows

$$g_{31} = \bar{g}_{31}(r) = g_0 e^{\lambda r} \tag{40}$$

where g_0 and λ are material constants and λ defines the graded property of the material. These parameters can be determined by the values of g_{31} at the inner and outer surfaces of the curved actuator, i.e.

$$\begin{cases} g_0 = g_{31}^i \left(\dfrac{g_{31}^i}{g_{31}^o}\right)^{\frac{R_1}{R_2 - R_1}} \\ \lambda = \dfrac{1}{R_2 - R_1}\ln\dfrac{g_{31}^o}{g_{31}^i} \end{cases} \tag{41}$$

in which g_{31}^i and g_{31}^o are the values of g_{31} in the inner and outer surfaces of the curved actuator, respectively. In terms of Taylor's series expansion theory, $\bar{g}_{31}(r)$ can be expanded as

$$\bar{g}_{31}(r) = g_0\left(1 + \lambda r + \frac{\lambda^2}{2!}r^2 + \frac{\lambda^3}{3!}r^3 + ... + \frac{\lambda^K}{K!}r^K + ...\right) \tag{42}$$

Here it can be seen that the coefficients $g_0\left(1, \lambda, \frac{\lambda^2}{2!}, \frac{\lambda^3}{3!}, ..., \frac{\lambda^K}{K!}...\right)$ correspond to the parameters $(J_0, J_1, J_2, J_3, \ldots, J_K\ldots)$ in Eq. (27), respectively.

In the following analysis, it is assumed that the inner and outer surfaces of the curved actuator are made of $BaTiO_3$ and PZT-4, respectively. So g_{31}^i and g_{31}^o can be taken to be g_{31}^i = -9.35×10^{-3} m^2/C and g_{31}^o = -17.8×10^{-3} m^2/C. Other material parameters of the actuator are listed in Table 1. Besides, R_1 and R_2 are taken to be 16 mm and 17.32 mm, respectively. The variations of the normal stresses (T_θ, T_r), the electrical potential ϕ and the electric displacement D_r with respect to the radius r are plotted in Figs. 9 to 12, respectively, under the external voltage V_0 = 100V and external load q = 10 kN/m^2.

The relationships between the analytical results of the displacement u_r and the radius r at V_0 = 100 V and q = 10 kN/m^2 are provided in Fig. 13. For comparison, numerical analysis obtained by

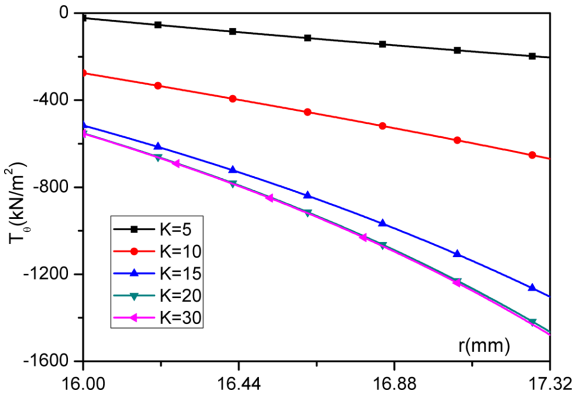

Fig. 9 Distribution of stress T_θ along radial direction

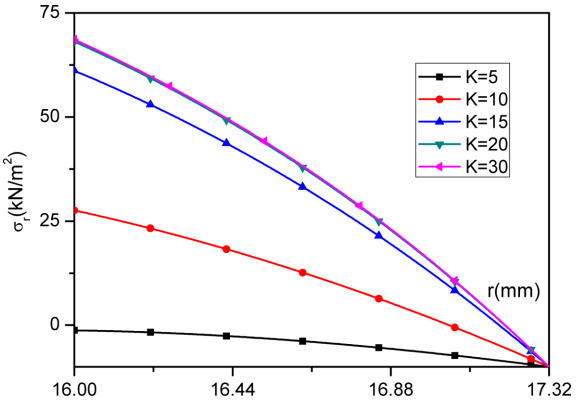

Fig. 10 Distribution of stress T_r along radial direction

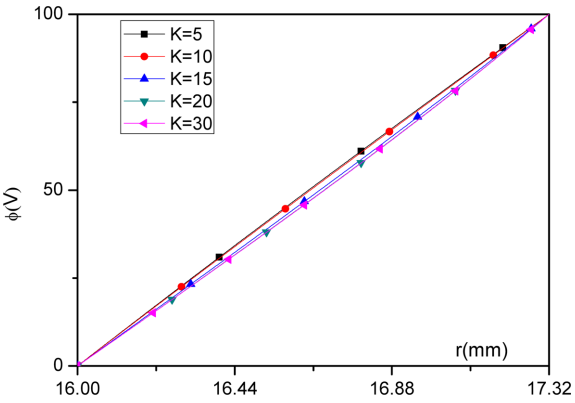

Fig. 11 Distribution of potential ϕ along radial direction

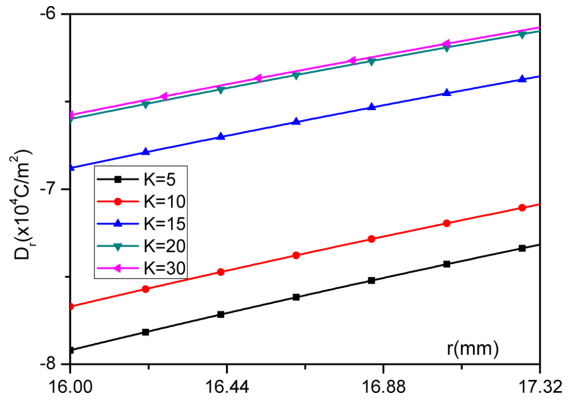

Fig. 12 Distribution of electric displacement D_r along radial direction

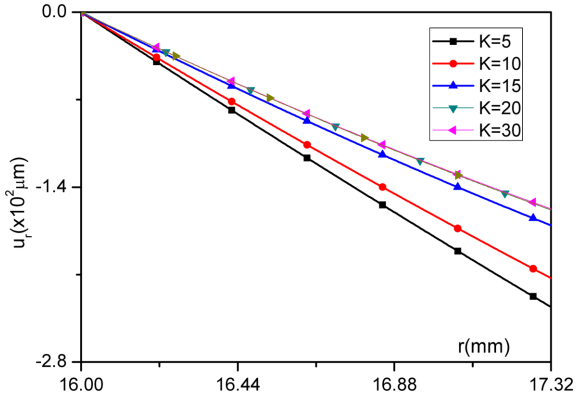

Fig. 13 Distribution of radial displacement u_r along radial direction

Ansys 9.0 with Solid 5 element is also plotted in Fig. 13. In numerical calculation, the distribution of g_{31} as shown in Eq. (40) is considered. These two figures demonstrate that the exact solutions obtained in the present paper agree very well with the FEM findings. These figures show that the curves of K = 15 and K = 20 are very close and the curve of K = 30 is almost superposed upon

the curve of $K = 20$. This indicates that the convergency of Eq. (28) is excellent. Besides, Figs. 9 and 10 show that the non-zero internal stresses (T_r, T_θ) always exist in the functionally graded curved actuator. The authors found that all the internal stresses will vanish in the linearly graded flat actuator when it was subjected to the external voltage (Hauke *et al*. (2000). Moreover, Figs. 11 and 12 show that both the electrical potential ϕ and the electric displacement D_r change almost linearly in the radial direction. Therefore, different distribution of g_{31} in radial direction only results in a slight change in the electric field E.

5. Conclusions

Based on the theory of elasticity, the analysis of multi-layered and continuously graded piezoelectric hollow cylinders showed in Figs. 1 and 8 is given and the exact solutions are obtained. In order to verify the validity of the solutions, the comparison between the two models is performed. In the continuous cylinder, the exact solutions given by Eq. (27) in the case of $K = 2$ is also plotted in Figs. 2-7. The subscript FGP (functionally graded piezoelectric) represents the exact solution in the continuous cylinder when $K = 2$. From the comparison, the following results can be found: (1) when cylinder is simultaneously subjected to the electric field and external load, T_r and T_θ will be non-zero in the FGP hollow cylinders. This is the major difference between the curved transducer and the flat transducer. Previous studies proved that there is not any stress component existing in the flat FGP transducer when it is subjected to the electric field. (2) The displacement u_r of the continuous cylinder is slightly larger than that of the multi-layered cylinder, the internal normal stresses of both cylinders are close. (3) Different distribution of the piezoelectric parameter g_{31} in radial direction does not cause major difference for the distribution of the electric field E. (4) The limit of the solutions of the multi-layered cylinder is consistent with that of the continuous cylinder as the number of layer increases.

Acknowledgements

This work is supported by the National Natural Science Foundation of China (50908007 and 50772010) and the Fundamental Research Funds for the Central Universities.

References

Angelino, M.R. and Washington, G.N. (2002), "Design and construction of a piezoelectric point actuated active aperture antenna", *J. Intel. Mat. Syst. Str*., **13**(2-3), 125-136.

Chaudhry, Z., Lalande, F. and Rogers, C.A. (1994), "Special considerations in the modeling of induced strain actuator patches bonded to shell structures", *Proc. SPIE,* **2190**, 563-570.

Crawley, E.F. (1994), "Intelligent structures for aerospace: a technology overview and assessment", *AIAA J.,* **32**(8), 1689-1699.

Hauke, T., Kouvatov, A., Steinhausen, R., Seifert, W., Beige, H., Langhammer, H.T. and Abicht, H.P. (2000), "Bending behavior of functionally gradient materials", *Ferroelectrics*, **238**(1), 195-202.

Ichinose, N., Miyamoto, N. and Takahashi, S. (2004), "Ultrasonic transducers with functionally graded piezoelectric ceramics", *J. Eur. Ceram. Soc.*, **24**(6), 1681-1685.

Ikeda, T. (1990), *Fundamentals of piezoelectricity*, Oxford University Press, USA.

Jayachandran, V., King, P., Meyer, N.E., Li, F.J., Petrova, M., Westervelt, M.A., Hirsh, S.M. and Sun, J.Q. (1999), "Real-time feedforward control of low-frequency interior noise using shallow spherical shell piezoceramic actuators", *Smart Mater. Struct.*, **8**(5), 579-584.

Kouvatov, A., Steinhausen, R., Seifert, W., Hauke, T., Langhammer, H.T., Beige, H. and Abicht, H.P. (1999), "Comparison between bimorphic and polymorphic bending devices", *J. Eur. Ceram. Soc*., **19**(6-7), 1153-1156.

Kruusing, A. (2000), "Analysis and optimization of loaded cantilever beam microactuators", *Smart Mater. Struct.*, **9**(2), 186-196.

Lalande, F., Chaudhry, Z. and Rogers, C.A. (1995), *An experimental study of the actuation authority of rings and shells*, AIAA Paper No. 95-1099.

Larson, P.H. and Vinson, J.R. (1993), "The use of piezoelectric materials in curved beams and rings", *Proceedings of the 1993 ASME Winter Annual Meeting*, New Orleans, LA, USA.

Liu, C.W. and Taciroglu, E. (2007), "Numerical analysis of end effects in laminated piezoelectric circular cylinders", *Comput. Method. Appl. M*., **196**(17-20), 2173-2186.

Liu, T.T. and Shi, Z.F. (2004), "Bending behavior of functionally gradient piezoelectric cantilever", *Ferroelectrics*, **308**, 43-51.

Marcus, M.A. (1984), "Performance characteristics of piezoelectric polymer flexure mode devices", *Ferroelectrics*, **57**(1-4), 203-220.

Rossi, A., Liang, C. and Rogers, C.A. (1993), "Impedance modeling of piezoelectric actuator-driven systems: an application to cylindrical ring structures", *Proceedings of the 34th AIAA/ASME/ASCE/AHS/ASC Structures*, La Jolla, CA, USA, April.

Ruan, X.P., Danforth, S.C., Safari, A. and Chou, T.W. (2000), "Saint-Venant end effects in piezoceramic materials", *Int. J. Solids Struct.*, **37**(19), 2625-2637.

Shi, Z.F. (2002), "General solution of a density functionally gradient piezoelectric cantilever and its applications", *Smart Mater. Struct.*, **11**(1), 122-129.

Shi, Z.F. (2005), "Bending behavior of piezoelectric curved actuator", *Smart Mater. Struct.*, **14**, 835-842.

Shi, Z.F. and Chen, Y. (2004), "Functionally graded piezoelectric cantilever under load", *Arch. Appl. Mech.*, **74**(3-4), 237-247.

Shi, Z.F. and Zhang, T.T. (2008), "Bending analysis of a piezoelectric curved actuator with a generally graded property for piezoelectric parameter", *Smart Mater. Struct.*, **17**(4), 045018 (7pp).

Sonti, V.R. and Jones, J.D. (1996), "Curved piezoactuator model for active vibration control of cylindrical shells", *AIAA J*., **34**(5), 1034-1040.

Taya, M., Almajid, A.A., Dunn, M. and Takahashi, H. (2003), "Design of bimorph piezo-composite actuators with functionally graded microstructure", *Sensor. Actuat. A-Phys.*, **107**, 248-260.

Tzou, H.S. and Gadre, M. (1989), "Theoretical analysis of a multi-layered thin shell coupled with piezoelectric actuators for distributed vibration controls", *J. Sound Vib*., **132**(3), 433-450.

Wu, C.C.M., Kahn, M. and Moy, W. (1996), "Piezoelectric ceramics with functional gradients: a new application in material design", *J. Am. Ceram. Soc.*, **79**(3), 809-812.

Yang, J.S. (2007), "One-dimensional equations for planar piezoelectric curved bars", *IEEE T. Ultrason. Ferr.*, **54**(10), 2202-2207.

Zhang, T.T. and Shi, Z.F. (2006), "Two-dimensional exact analysis for piezoelectric curved actuators", *J. Micromech. Microeng.*, **16**(3), 640-647.

Zhu, X.H. and Meng, Z.Y. (1995), "Operational principle, fabrication and displacement characteristic of a functionally gradient piezoelectric ceramic actuator", *Sensor. Actuat. A-Phys.*, **48**(3), 169-176.

BS